How to cite: *Angew. Chem. Int. Ed.* **2022,** *61,* e202212293
International Edition: doi.org/10.1002/anie.202212293
German Edition: doi.org/10.1002/ange.202212293

Circulenes Hot Paper

Electronic Materials: An Antiaromatic Propeller Made from the Four-Fold Fusion of Tetraoxa[8]circulene and Perylene Diimides

Viktor B. R. Pedersen, Stephan K. Pedersen, Zexin Jin, Nicolaj Kofod, Bo W. Laursen, Glib V. Baryshnikov, Colin Nuckolls,* and Michael Pittelkow**

Abstract: The synthesis of an antiaromatic tetraoxa-[8]circulene annulated with four perylene diimides (PDI), giving a dynamic non-planar π-conjugated system, is described. The molecule contains 32 aromatic rings surrounding one formally antiaromatic planarized cyclooctatetraene (COT). The intense absorption ($\varepsilon = 3.35\times10^5\ M^{-1}cm^{-1}$ in CH_2Cl_2) and emission bands are assigned to internal charge-transfer transitions in the combined PDI-circulene π-system. The spectroscopic data is supported by density functional theory calculations, and nuclear independent chemical shift calculation indicate that the antiaromatic COT has increased aromaticity in the reduced state. Electrochemical studies show that the compound can reversibly reach the tetra- and octa-anionic states by reduction of the four PDI units, and the deca-anionic state by reduction of the central COT ring. The material functions effectively in bulk hetero junction solar cells as a non-fullerene acceptor, reaching a power conversion efficiency of 6.4 %.

Introduction

Exploration of the available chemical space for fully conjugated nano-graphene structures beyond planar all-carbon/all-hexagon structures is an attractive strategy to access tailor made molecules with unique properties.[1] Geometric constraints of the internal conjugated rings and of the overall π-conjugated system influence properties such as chirality due to restricted rotation or embedded helicenes and often lead to enhanced solubility and processability.[2] Examples encompass so-called warped nano-graphenes and molecules with other types of curved conjugated surfaces, including bowl-shaped molecules such as corannulene.[3–5]

Aromatic molecules generally obey the Hückel's Rule of $4n+2$ for cyclic conjugated π-electrons, while antiaromatic molecules exist in the $4n$ π-electron regime.[6–8] Antiaromatic molecules are often characterized by lower chemical stability than aromatic molecules, and tend to alleviate the energetically disfavored antiaromatic nature by deviating from planarity or by distorting bond lengths.[9,10] The introduction of antiaromatic moieties in larger π-conjugated structures or by coordination to transition metals are viable strategies to stabilize the antiaromatic units and to tailor the properties of the larger π-conjugated structure.[11] Antiaromatic molecules often have low HOMO–LUMO gaps, making them attractive in light emitting devices.[12] Elegant examples of stabilized antiaromatic units are π-extended indenofluorenes and norcorroles.[1a,13–18]

To fully harness the power of antiaromaticity in the context of π-conjugated molecules, the development of new synthetic methodologies is a key challenge. Recent years have witnessed the description of a range of strategies to prepare molecules of the heterocyclic [8]circulene type.[19–25] A number of these structures are chemically stable, planar and contain an antiaromatic cyclooctatetraene (COT) unit.[26] The all-carbon [8]circulene has also been prepared, and this has a saddle shape geometry, thus highlighting the importance of the heteroatoms in dictating the molecular geometry.[27]

The parent tetraoxa[8]circulene (**3**) is highly insoluble in most solvents and is purified by sublimation, but its synthetic availability in only two steps, makes it an attractive platform for the exploration of this antiaromatic motif.[28] It is especially worth mentioning that the formation of tetraoxa-[8]circulenes from substituted 1,4-benzoquinones do not tend to work using 1,4-benzoquinones bearing electron

[*] V. B. R. Pedersen, Dr. S. K. Pedersen, N. Kofod, Prof. Dr. B. W. Laursen, Prof. Dr. M. Pittelkow
Department of Chemistry,
University of Copenhagen
Universitetsparken 5, 2100 Copenhagen Ø (Denmark)
E-mail: pittel@chem.ku.dk
Dr. Z. Jin, Prof. Dr. C. Nuckolls
Department of Chemistry,
Columbia University
3000 Broadway, New York, NY (USA)
E-mail: cn37@columbia.edu
Prof. Dr. G. V. Baryshnikov
Department of Science and Technology, Laboratory of Organic Electronics,
Linköping University
Norrköping, SE-60174 (Sweden)
E-mail: glib.baryshnikov@liu.se

accepting properties, thus rendering electron deficient tetraoxa[8]circulenes unexplored. The inherent electron accepting properties and the high stability of PDIs have made them interesting building blocks for a range of compounds for organic photovoltaics (OPVs).[29–31] Organic scaffolds containing PDIs have found interest in recent years as electron acceptors for non-fullerene organic solar cells.[32] The strong absorption and emission of PDIs in the visible range have made them viable candidates for optoelectronic applications. Their electronic and optical properties can be tuned by substitution on the periphery of PDI, and have the possibility of production on a larger scale compared to fullerenes, with the latter being a commonly employed electron acceptor in OPVs.[33] PDI-derivatives have shown high electron mobility and efficient photo-induced charge separation, which are important contributing properties for bulk heterojunction (BHJ) organic solar cells.[34] When employed in BHJ organic solar cells, PDI-derivatives have shown a high degree of self-aggregation, leading to low power conversion efficiencies (PCE). A way to overcome the self-aggregation is to introduce a twisted non-planar structure into the PDI-scaffold.[30,35–40]

Herein we demonstrate for the first time how the attractive properties of tetraoxa[8]circulene and PDIs can be harnessed in a single system. By annulating four PDIs to a single tetraoxa[8]circulene unit, a voluminous non-planar conjugate, centered around a COT, with 32 annulated aromatic rings is formed. The electron withdrawing nature of the PDIs enable the electrochemical observation of the reduction of the COT to the decaanionic species. The compound is highly soluble due to the non-planar structure and the eight lateral alkyl-chains. As a non-fullerene acceptor in BHJ solar cells, this molecule performs with a power conversion efficiency of 6.4 %.

Results and Discussion

Iridium catalyzed borylation of the poorly soluble unsubstituted tetraoxa[8]circulene (**3**) yields a soluble tetraborylated tetraoxa[8]circulene (**4**), with one borylation per benzene ring in a non-regiospecific manner. The propeller (**1**, Scheme 1) was synthesized utilizing a Suzuki cross-coupling between tetraoxa[8]circulene **4** and PDI **5a** precursors, followed by an oxidative photocyclization, yielding compound **1** in 22 % yield over two steps. The central core formally exhibits 8π antiaromaticity, and the four PDI-units acts as "wings" of the propeller (see wings in red, Scheme 1). By design the physical size of the PDI-units will inevitably overlap, leading to a twisted structure which hinders self-aggregation. The twisted structure could potentially lead to a range of different stereoisomers due to the presence of, in principle, four stereogenic axes and their sterically restricted interconversion (Figure S9). Analysis of the NMR spectra reveal only one highly symmetrical isomer. Investigation of this material using HPLC on a chiral stationary phase yielded two separated peaks (see Figure S10). Upon collection of these separated peaks, followed by reinjection to the column lead to the reobservation of two isomers, indicating a dynamic racemization process at room temperature.[41] The highly symmetrical ^{1}H NMR spectrum (Figure S1) reveal that these two stereoisomers

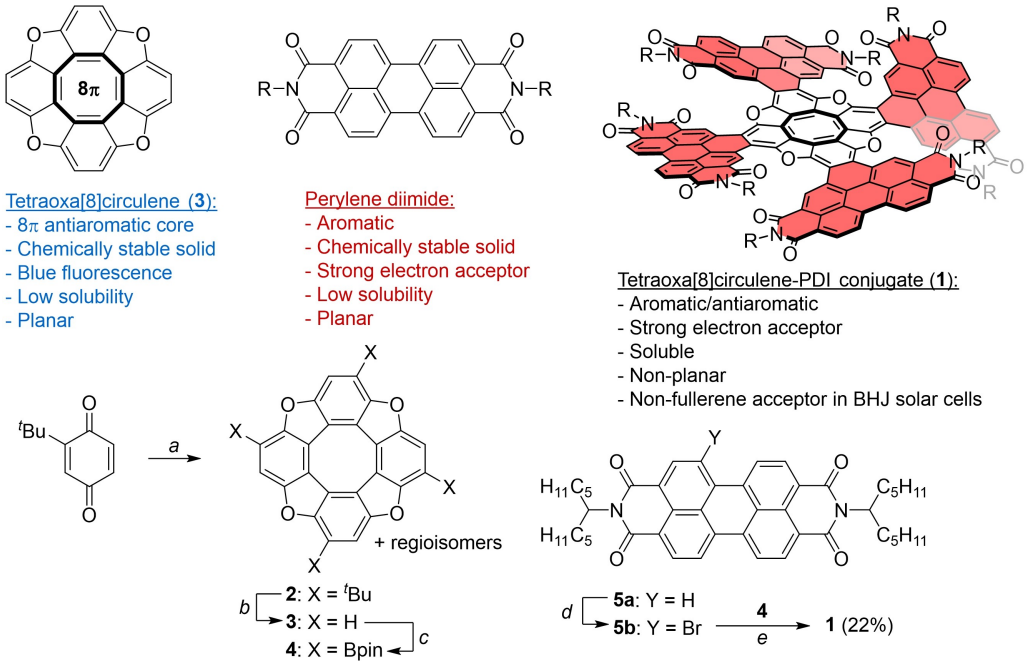

Scheme 1. Synthesis of compound **1**. a) $BF_3{\cdot}Et_2O$, CH_2Cl_2, 50 %. b) $AlCl_3$, benzene, overnight, 99 %. c) [Ir(OMe)(1,5-cod)]$_2$, bis(pinacolato)diboron, 4,4′-di-tert-butyl-2,2′-bipyridine, cyclohexane, 80 °C, 19 h, 95 %. d) Br_2, CH_2Cl_2, overnight, 30 %. e) 1) Pd(dppf)$Cl_2{\cdot}CH_2Cl_2$, Cs_2CO_3, PhMe/H_2O, 50 °C, 16 h. 2). I_2, hν, PhMe, 16 h. 22 % over two steps.

have identical spectra. This agrees with the "propeller"-like, all *M* or all *P* at the four axes of chirality, conformer of **1** of D_4 symmetry, as illustrated in Scheme 1. Two other conformational isomers of compound **1** exists, of D_{2d} and C_2 symmetry (Figure S9). The presence of these can, however, be excluded based on the simplicity of the ^{1}H NMR spectrum (C_2) or from the chiral HPLC (D_{2d}) due to the achirality of the D_{2d} conformer. Furthermore, the observation of them by NMR spectroscopy, or lack thereof, is supported by the calculated energy difference relative to the 'propeller'-like conformer of 2.9 and 6.6 kcal mol^{-1} for the C_2 and D_{2d} conformation isomers, respectively.

We then considered the racemization pathway of compound **1** (conformer A) through the stepwise mechanism: A ↔TS1↔C↔TS2↔B (TS = transition state, Figure S11). The key stage of racemization is a transformation between the chiral conformer C and achiral conformer B. At this stage the mirror inversion happens because of the structure of transition state TS2 between C and B conformers allows the equal probability to transit into the left and right-handed enantiomers of conformer C and then of conformer A. Our calculations predict the rate determining stage of racemization at TS2 step and the barrier height (relative to the ground state conformation A) is 19.9 and 24.5 kcal mol^{-1} at AM1 and B3LYP/6-31G(d) levels of theory, respectively (Figure S11), indicating that racemization close to room temperature is viable.

UV/Vis absorption spectra of compounds **1**, **2** and **5a** along with the emission spectrum of **1** in toluene are shown in Figure 1. Compound **1** showed a strong absorption band at 441 nm, with a very high molar extinction coefficient of 2.90×10^5 M^{-1}cm^{-1} in toluene. It is clear from Figure 1 that the optical spectrum of **1** is very different from those of the circulene (**2**) and PDI (**5a**) precursors. DFT calculations explain the intense absorption at 441 nm by two sets of degenerate intramolecular charge-transfer transitions. The first set (HOMO→LUMO+4 and HOMO-1→LUMO+4) is a charge-transfer transition from the degenerate HOMO orbitals mostly located on the PDI units (see Figure 2) with some circulene character to the LUMO+4 orbital exclusively located on circulene (Figure S14). Conversely, the second set (HOMO-5→LUMO and HOMO-6→LUMO) is a charge-transfer transition from mostly circulene with some PDI character to the LUMO with exclusive PDI character (see detailed analysis in the Supporting Information (S24 and Figure S14)). These highly altered optical properties led us to perform a more detailed photophysical characterization of **1**, of which the properties are summarized in Table 1. Invariant excitation spectra across multiple emission wavelengths (Figure S24) match the absorption spectrum (Figure S22), proving that the emission spectrum (Figure S22, S23) originates from only one emitter, that is also responsible for the full absorption spectrum. No signs of any significant impurities or sample/conformational inhomogeneity is observed.

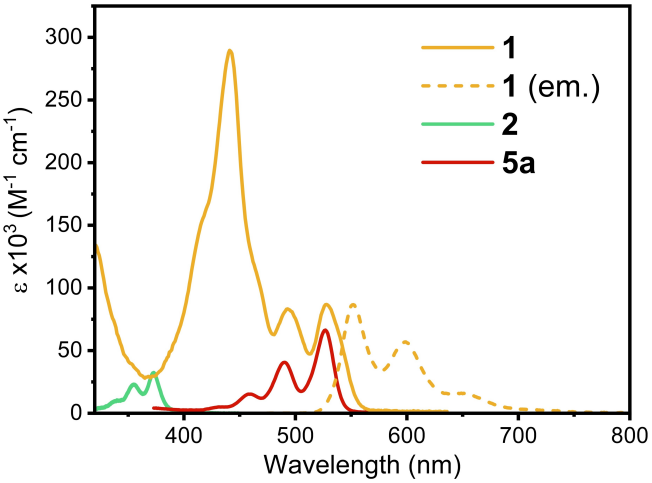

Figure 1. UV/Vis absorption spectra of compounds **1**, **2** and **5a**, and emission spectrum of **1**. Spectra were recorded in toluene at room temperature (absorption) or 20 °C (emission).

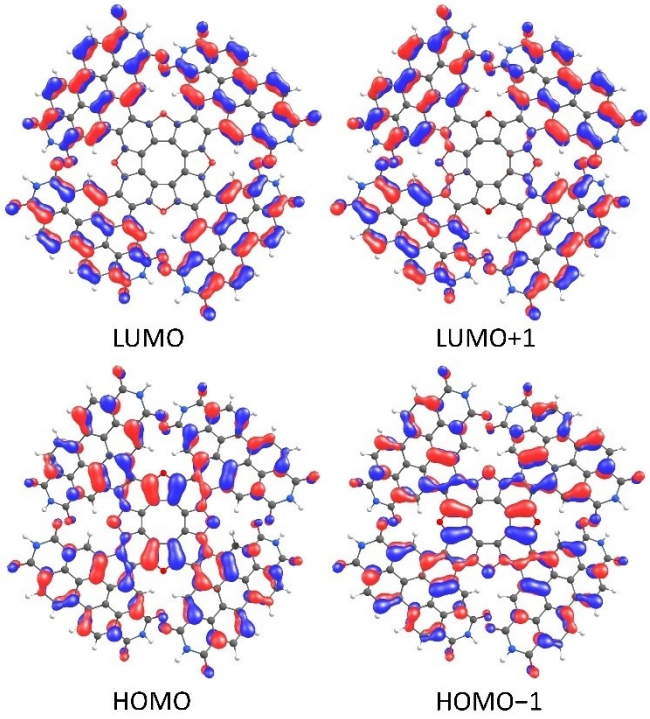

Figure 2. Frontier molecular orbitals of compound **1**. HOMO, HOMO-1 and LUMO, LUMO+1 wavefunctions are pairwise degenerated within D_4 symmetry point group. Alkyl chains have been replaced with hydrogens.

Table 1: Photophysical parameters.[a]

Solvent	Φ_f[b] [%]	τ_{obs} [ns]	k_f [$\times10^7$ s^{-1}][c]	k_{nr} [$\times10^7$ s^{-1}][d]	$\varepsilon_{438\,nm}$ [$\times10^3$ M^{-1} cm^{-1}]
CH_2Cl_2	16	8.47	1.9	9.9	335
Toluene	29	7.23	4.1	9.8	290

[a] Determined at 20 °C, using coumarin 153 as a reference in absolute ethanol ($\Phi_f = 0.53\pm0.04$). [b] Fluorescence quantum yield. [c] Rate of fluorescence. [d] Rate of non-radiative decay.

The emission spectrum of **1** in toluene is remarkably similar to that of simple PDI (**5a**), showing the same vibrational fine-structure, just red shifted around 440 cm^{-1} (Figures S26, S27). However, the fluorescence lifetime of **1** (7.23 ns)[42] is almost twice that of PDI (**5a**) (4.03 ns) (Figures S44, S45) indicating a much lower rate of fluorescence, k_f. This was confirmed by determining the fluorescence quantum yield of PDI (**5a**) and **1** (Table S2). The quantum yield of PDI (**5a**) in CH_2Cl_2 is 81 % while the quantum yield of **1** in toluene is only 29 %. This is also reflected in the k_f and oscillator strengths (Table S2) where **1** is a factor of 5 lower than that of PDI (**5a**). From this we can conclude that while the emission of **1** in toluene looks like that of PDI (**5a**) it most certainly is not originating from a simple local transition on a PDI unit. Instead, this all points to— a very weak transition between ground and first excited state. This is also indicated in the non-Gaussian red-edge of the absorption spectrum that differs from the simple PDI (Figure S25).

DFT Calculations show that first excited state (S_1) for compound **1** (within D_4 symmetry point group) is doubly degenerated and is a charge transfer (CT) transition from the circulene to the PDI moieties. Degeneration of S1 (HOMO–LUMO configuration) and S_2 (HOMO-1-LUMO configuration) states (both of E symmetry) occurs due to the degeneracy of the HOMO and HOMO-1 orbitals (Figure 2). Both HOMO and HOMO-1 wavefunctions are localized mainly on the inner tetraoxa[8]circulene core with considerable contributions of PDI fragments, while LUMO is equally distributed over the four PDI branches without any amplitude on central circulene core (Figure 2).

The intensity of both S_0–S_1 and S_0–S_2 electronic transitions is very small ($f = 3 \times 10^{-4}$), which, when accounting for explicit solvent effects, intermolecular interactions and symmetry breaking could be one-two orders of magnitude higher. One should note, that population of such centrosymmetric CT states does not lead to the change of molecular permanent dipole moment. This predicts insensitivity of their energy to solvent polarity, in agreement with experimental spectra (Figure S29). It seems that this is a general property of symmetrical compounds sustaining centrosymmetric CT states. Similar solvent-independent behavior of absorption spectra was also observed for symmetrical hexaphenoxy-, hexakis(phenylthio)-, and hexakis(phenylselanyl)benzenes.[43] We find good agreement between calculated transitions and the experimental spectra (Figure S30), all pointing to photophysical properties dominated by the weakly allowed, yet surprisingly emissive, CT transitions involving the entire π-system.

Going from toluene to CH_2Cl_2 the vibrational fine-structure of the emission spectra is completely lost (Figure S29). Arguably, this could simply be due to aggregation. However, time-resolved anisotropy (Figures S48–S50, summarized in Table S4) show rotational correlation times of compound **1** of 1.029 ns and 0.734 ns in toluene and CH_2Cl_2 respectively. This is compared to a rotational correlation time of 0.27 ns of PDI (**5a**). Using the Perrin equation, we correlate the rotational correlation times to molecular volumes. The molecular volume of **1** is comparable in toluene and CH_2Cl_2 at 67–75 nm^3, and approximately 4 times bigger than that of PDI (**5a**) (19–20 nm^3). This confirms the significant size of the **1** molecule and show that the loss of fine structure is not due to aggregation.

Similar observations of solvent-dependent vibronic progression were described for dianthracenylazatrioxa-[8]circulene compound which demonstrates well resolved fine structure in fluorescence spectrum measured in toluene with longer emission lifetime, and no resolved fine structure in CH_2Cl_2 with shorter emission lifetime.[44] Based on quantum-chemical calculations it was assumed that solvent dependence of vibronic fluorescence originates from polarity-dependent derivatives of the transition dipole moment between the initial and final states due to the asymmetrical displacement vectors of corresponding vibrational modes active in Herzberg-Teller progression.

Surprisingly, the absorption and fluorescence of solid-state samples, as thin film and powder, are quite similar to that of the CH_2Cl_2 solution (Figure S51, S52 and Table S3). The small red-shift observed going from CH_2Cl_2 to thin film and powder is assigned to effects of the dielectric environment and self-absorption.[45] This indicates that no strong electronic coupling occurs despite the close packing of chromophores, as is otherwise most often the case for PDI's in the solid state. This is likely due to the contorted structure and branched side chains of compound **1**, which prohibits such interactions.[46]

It is well known that PDI-units can accept two electrons in stepwise reductions, thus we wanted to investigate the electrochemical properties of compound **1**.[29,31,47] Furthermore, the formation of a Hückel 10π aromatic central core have previously been suggested by reduction of tetraoxa-[8]circulene. Cyclic and differential pulse voltammograms of **1** are shown in Figure 3. For other systems containing multiple PDI-fragments simultaneous reductions are observed for equivalent PDIs, leading to multiple electron

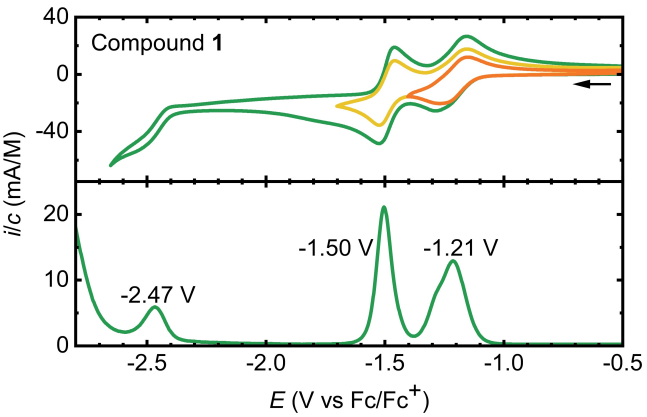

Figure 3. Top: Cyclic voltammograms of compound **1**. All potentials are depicted against the Fc/Fc^+ redox couple. Orange: Scanned from −0.35 to −1.40 V. Yellow: Scanned from −0.35 to −1.70 V, Green: Scanned from −0.35 to −2.65 V. Bottom: Differential pulse voltammogram. Voltammograms were recorded in CH_2Cl_2 at 0.5 mM; supporting electrolyte: 0.1 M Bu_4NPF_6, scan rates: 0.1 $V s^{-1}$ for CVs, 0.004 $V s^{-1}$ for the DPV.

reductions at given potentials.[29] The electrochemistry of **1** revealed two reversible four-electron reductions leading to the formations of the tetra- and octaanion at −1.21 and −1.50 V vs Fc/Fc^+, respectively. This suggest that the four equivalent PDIs are reduced together in a stepwise manner independently of each other in reversible processes to form the tetra- and octaanions. An irreversible two-electron reduction was observed at −2.47 V vs Fc/Fc^+ which we assign to the reduction of the central tetraoxa[8]circulene core, in good correlation to the reduction potential of tetraoxa[8]circulene **2** at −2.36 V vs Fc/Fc^+ (Figure S55).

In order to investigate the change in aromaticity of compound **1** and to probe the formally antiaromatic core when it undergoes reductions, we performed nuclear independence chemical shift (NICS) and anisotropy of induced current density (ACID) calculations of the neutral, cationic (+2) and anionic (−2, −4, −6, −8, −10) species, along with the neutral, cationic (+2) and anionic (−2) species of compound **3** and neutral and anions (−, −2) of PDI (see Figure 4 and Figure S19–S21). A switching from antiaromatic to aromatic character of the central core of tetraoxa[8]circulene **3** is observed in the dianionic state (Figures S17). We expected that a significant amount of the negative charge for the tetra- and octaanions would be situated on the highly electron accepting PDI-moieties, and indeed no change in the aromaticity of the central core was observed for these species as follows from both NICS and ACID calculations. The decaanion of **1** showed a change in the aromaticity of central core which becomes aromatic, as follows from ACID plot (Figure 4 and Figure S21), though one could imagine the two electrons could be situated around the central core, mimicking the aromaticity of dianionic tetraoxa[8]circulene $\mathbf{3}^{2-}$ (Figure 4). This correlates well with the observed irreversible reduction to the deca-

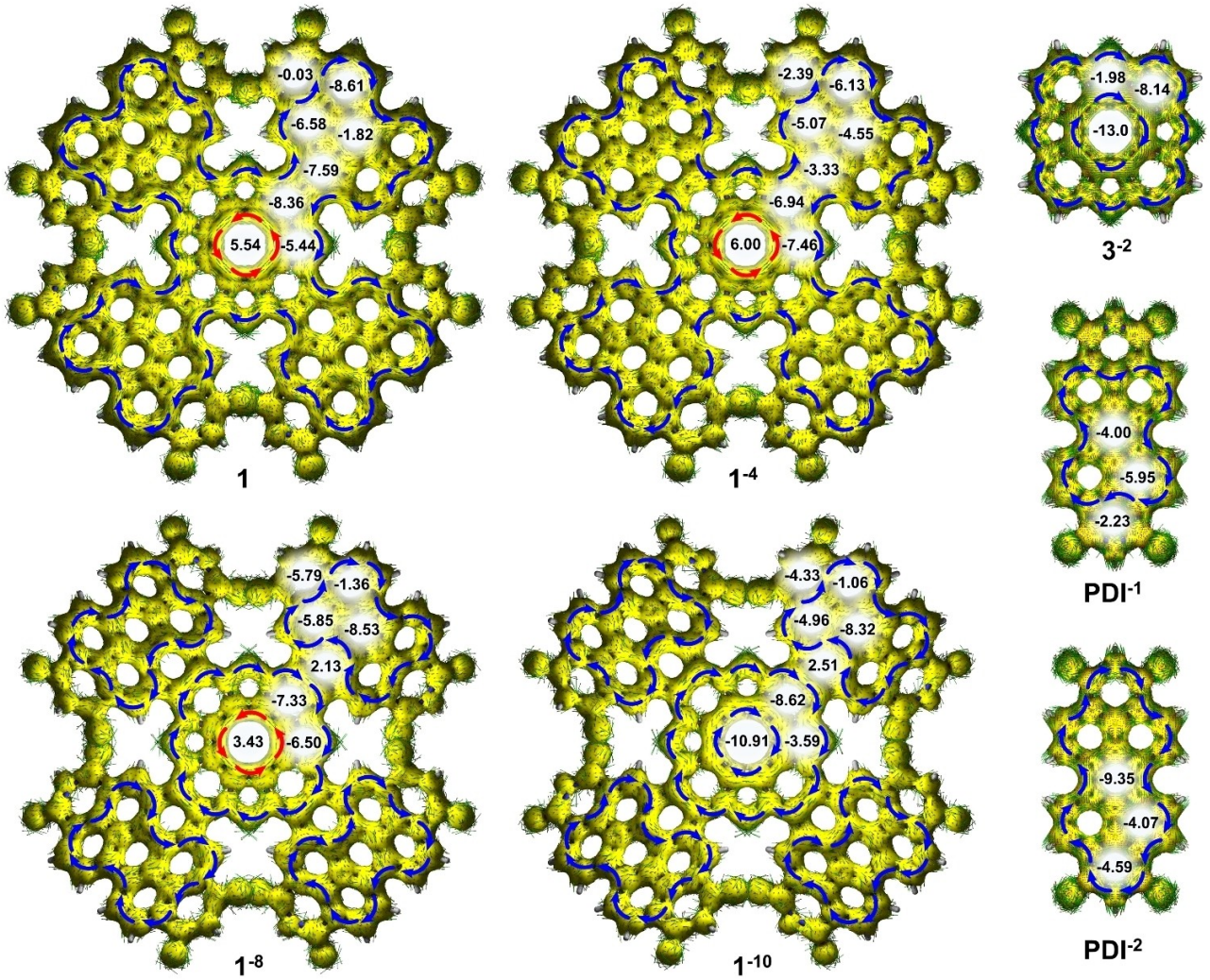

Figure 4. Calculated ACID plots for neutral and anionic (−4, −8, −10) species of compound 1, dianonic tetraoxa[8]circulene 3 as well as mono- and dianonic species of simple PDI. Calculated NICS(1) values for all compounds are shown in the figure in bold, as the value in the center of the ring. NICS(1) values for rings related by symmetry are not shown. NICS(0) values, as well as NICS(1) values for other neutral and ionic species can be found in the Supporting Information (Figure S17). ACID plots for neutral (PDI and 3) and other ionic species (1: (−2, −6), 3: (+2)) can be found in the Supporting Information (Figure S19–S21).

anion at the significantly lower potential (−2.47 V vs Fc/Fc^+).

The high chemical stability of **1**, combined with the attractive optical properties encouraged us to investigate this as a non-fullerene acceptor in organic photovoltaics OPV. PTB7-Th[48,49] was chosen as the corresponding electron donor to form the active layer with **1**, due to its high performance in both fullerene- and nonfullerene-based solar cells. We fabricated bulk heterojunction (BHJ) solar cell devices in an inverted configuration[50] of ITO/ZnO (20 nm)/PTB7-Th:**1**/MoO_3 (7 nm)/Ag (90 nm). The optimization of the solar cells (such as varying the ratio of donor and acceptor, the additives, and thermal annealing) are detailed in the Supporting Information, Table S5. Figure 5 shows the EQE spectrum and current density *J–V* curve of the highest performance cell. The photovoltaic parameters are summarized in Table 2. Remarkably the cell exbibits a PCE of 6.4 % with a photocurrent density of 14.2 mA cm^{-2} and a photovoltage of 0.87 V. This performance of the cells fabricated from compound **1** is among the top rank of PDI-based materials.[51]

Conclusion

To summarize, we have successfully synthesized and characterized a "propeller"-like molecule consisting of a tetraoxa-[8]circulene core with four annulated PDI-units. The compound shows very strong absorption bands in the visible spectrum with a molar extinction coefficient of 290 × 10^3 M^{-1} cm^{-1} at 441 nm in toluene. A symmetric circulene to PDI charge transfer transition results in fluorescence at 552 nm with a quantum yield of 29 % and a fluorescence lifetime of 4.03 ns in toluene. Tetra- and octaanions of **1** were reversibly reached through electrochemical reductions, suggesting two stepwise four-electron reduction indicating that all four PDIs acts independently of each other. The functionalization of the tetraoxa[8]circulene core with the four electron withdrawing PDI units further allowed the first experimental observation of the 10π-aromatic COT. Finally, the molecular architecture incorporating an antiaromatic ring in a non-fullerene acceptor for BHJ solar cells highlights a bright future for combined aromatic/antiaromatic molecules.

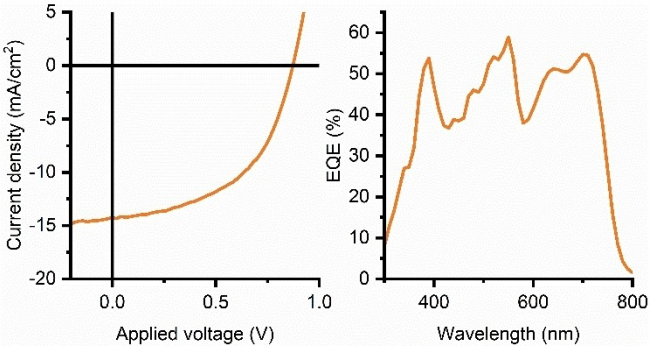

Figure 5. Left: Current density curve. Right: EQE spectrum.

Table 2: Photovoltaic parameters.

J_{sc} [mA cm^{-2}]	V_{oc} [V]	FF	PCE [%]	J_{sc} [mA cm^{-2}]
14.2	0.87	0.52	6.4	14.2

Acknowledgements

M.P. appreciate the support from the Danish Council for Independent Research (DFF 4181-00206 and 9040-00265) and from the University of Copenhagen. G.B. acknowledges the financial support of the Swedish Research Council (Starting Grant No. 2020-04600). The quantum-chemical calculations were performed with computational resources provided by the Swedish National Infrastructure for Computing (SNIC 2021-3-22) at the High-Performance Computing Center North (HPC2N) partially funded by the Swedish Research Council through Grant Agreement No. 2018-05973. We thank Prof. Ole Hammerich for insightful discussions. C.N. thanks Sheldon and Dorothea Buckler for their generous support.

Conflict of Interest

The authors declare no conflict of interest.

Data Availability Statement

The data that support the findings of this study are available from the corresponding author upon reasonable request.

Keywords: Antiaromaticity · Aromaticity · DFT · Solar Cells · Spectroscopy

[1] a) K. Kawasumi, O. Zhang, Y. Segawa, L. T. Scott, K. Itami, *Nat. Chem.* **2013**, *5*, 739–744; b) S. Pun, Q. Miao, *Acc. Chem. Res.* **2018**, *51*, 1630–1642; c) G. González Miera, S. Matsubara, H. Kono, K. Murakami, K. Itami, *Chem. Sci.* **2022**, *13*, 1848–1868; d) Chaolumen, I. Stepek, K. Yamada, H. Ito, K. Itami, *Angew. Chem. Int. Ed.* **2021**, *60*, 23508–23532; *Angew. Chem.* **2021**, *133*, 23700–23724.
[2] I. R. Márquez, S. Castro-Fernández, A. Millán, A. G. Campaña, *Chem. Commun.* **2018**, *54*, 6705–6718.
[3] J. I. Urgel, M. D. Giovannantonio, Y. Segawa, P. Ruffieux, L. T. Scott, C. A. Pignedoli, K. Itami, R. Fasel, *J. Am. Chem. Soc.* **2019**, *141*, 13158–13164.
[4] A. Escayola, A. Poater, A. Muñoz-Castro, M. Solá, *Chem. Commun.* **2021**, *57*, 3087–3090.
[5] H.-A. Lin, Y. Sato, Y. Segawa, T. Nishihara, N. Sugimoto, L. T. Scott, T. Higashiyama, K. Itami, *Angew. Chem. Int. Ed.* **2018**, *57*, 2874–2878; *Angew. Chem.* **2018**, *130*, 2924–2928.
[6] E. Hückel, *Z. Phys.* **1931**, *70*, 204–286.
[7] R. Breslow, *Acc. Chem. Res.* **1973**, *6*, 393–398.
[8] Z. Zeng, X. Shi, C. Chi, J. T. L. Navarrete, J. Casado, J. Wu, *Chem. Soc. Rev.* **2015**, *44*, 6578–6596.
[9] R. Breslow, *Chem. Rec.* **2014**, *14*, 1174–1182.

[10] S. K. Pedersen, K. Eriksen, H. Aagren, B. F. Minaev, N. N. Karaush-Karmazin, O. Hammerich, G. V. Baryshnikov, M. Pittelkow, *J. Am. Chem. Soc.* **2020**, *142*, 14058–14063.
[11] X.-Y. Wang, M. Richter, Y. He, J. Björk, A. Riss, R. Rajesh, M. Garnica, F. Hennersdorf, J. J. Weigand, A. Narita, R. Berger, X. Feng, W. Auwärter, J. V. Barth, C.-A. Palma, K. Müllen, *Nat. Commun.* **2017**, *8*, 1948.
[12] K. B. Ivaniuk, G. V. Baryshnikov, P. Y. Stakhira, S. K. Pedersen, M. Pittelkow, A. Lazauskas, D. Volyniuk, J. V. Grazulevivius, B. F. Minaev, H. Ågren, *J. Mater. Chem. C* **2017**, *5*, 4123–4128.
[13] D. T. Chase, B. D. Rose, S. P. McClintock, L. N. Zakharov, M. M. Haley, *Angew. Chem. Int. Ed.* **2011**, *50*, 1127–1130; *Angew. Chem.* **2011**, *123*, 1159–1162.
[14] T. Ito, Y. Hayashi, S. Shimizu, J. Y. Shin, N. Kobayashi, H. Shinokubo, *Angew. Chem. Int. Ed.* **2012**, *51*, 8542–8545; *Angew. Chem.* **2012**, *124*, 8670–8673.
[15] M. Yamashina, Y. Tanaka, R. Lavendomme, T. Ronson, M. Pittelkow, J. R. Nitschke, *Nature* **2019**, *574*, 511–514.
[16] A. Rajca, A. Safronov, S. Rajca, J. Wongsriratanakul, *J. Am. Chem. Soc.* **2000**, *122*, 3351–3357.
[17] J. Urieta-Mora, M. Krug, W. Alex, J. Perles, I. Fernández, A. Molina-Ontoria, D. Guldi, N. Martín, *J. Am. Chem. Soc.* **2020**, *142*, 4162–4172.
[18] Y. Tobe, S. Nobusue, *Synlett* **2016**, *27*, 2140–2144.
[19] T. Hensel, N. N. Andersen, M. Plesner, M. Pittelkow, *Synlett* **2015**, *27*, 498–525.
[20] S. Kato, Y. Serizawa, D. Sakamaki, S. Seki, Y. Miyake, H. Shinokubo, *Chem. Commun.* **2015**, *51*, 16944–16945.
[21] X. Xiong, C.-L. Deng, B. F. Minaev, G. V. Baryshnikov, X.-S. Peng, H. N. C. Wong, *Chem. Asian J.* **2015**, *10*, 969–975.
[22] F. Chen, Y. S. Hong, D. Kim, T. Tanaka, A. Osuka, *ChemPlusChem* **2017**, *82*, 1048–1051.
[23] C. Feng, M. Kuo, Y. Wu, *Angew. Chem. Int. Ed.* **2013**, *52*, 7791–7794; *Angew. Chem.* **2013**, *125*, 7945–7948.
[24] P. An, R. Li, B. Ma, R. He, Y. Zhang, M. Xiao, B. Zhang, *Angew. Chem. Int. Ed.* **2021**, *60*, 24478–24483; *Angew. Chem.* **2021**, *133*, 24683–24688.
[25] R. Dubey, M. Melle-Franco, A. Mateo-Alonso, *J. Am. Chem. Soc.* **2022**, *144*, 2765–2774.
[26] Y. Miyake, H. Shinokubo, *Chem. Commun.* **2020**, *56*, 15605–15614.
[27] Y. Sakamoto, T. Suzuki, *J. Am. Chem. Soc.* **2013**, *135*, 14074–14077.
[28] T. Brock-Nannestad, C. B. Nielsen, M. Schau-Magnussen, P. Hammershøj, T. K. Reenberg, A. B. Petersen, D. Trpcevski, M. Pittelkow, *Eur. J. Org. Chem.* **2011**, 6320–6325.
[29] S. R. Peurifoy, E. Castro, F. Liu, X. Y. Zhu, F. Ng, S. Jockusch, M. L. Steigerwald, L. Echegoyen, C. Nuckolls, T. J. Sisto, *J. Am. Chem. Soc.* **2018**, *140*, 9341–9345.
[30] Y. Zhong, M. T. Trinh, R. Chen, G. E. Purdum, P. P. Khlyabich, M. Sezen, S. Oh, H. Zhu, B. Fowler, B. Zhang, W. Wang, C. Y. Nam, M. Y. Sfeir, C. T. Black, M. L. Steigerwald, Y. L. Loo, F. Ng, X. Y. Zhu, C. Nuckolls, *Nat. Commun.* **2015**, *6*, 8242.
[31] E. Castro, T. J. Sisto, E. L. Romero, F. Liu, S. R. Peurifoy, J. Wang, X. Zhu, C. Nuckolls, L. Echegoyen, *Angew. Chem. Int. Ed.* **2017**, *56*, 14648–14652; *Angew. Chem.* **2017**, *129*, 14840–14844.
[32] J. Zhang, H. S. Tan, X. Guo, A. Facchetti, H. Yan, *Nat. Energy* **2018**, *3*, 720–731.
[33] R. Ganesamoorthy, G. Sathiyan, P. Sakthivel, *Sol. Energy Mater. Sol. Cells* **2017**, *161*, 102–148.
[34] M. Kim, S. U. Ryu, S. A. Park, Y.-J. Pu, T. Park, *Chem. Sci.* **2021**, *12*, 14004–14023.
[35] F. Saal, F. Zhang, M. Holzapfel, M. Stolte, E. Michail, M. Moos, A. Schmiedel, A.-M. Krause, C. Lambert, F. Würthner, P. J. Ravat, *J. Am. Chem. Soc.* **2020**, *142*, 21298–21303.
[36] G. Liu, T. Koch, Y. Li, N. L. Doltsinis, Z. Wang, *Angew. Chem. Int. Ed.* **2019**, *58*, 178–183; *Angew. Chem.* **2019**, *131*, 184–189.
[37] C. Yan, S. Barlow, Z. Wang, H. Yan, A. K. Y. Jen, S. R. Marder, X. Zhan, *Nat. Rev. Mater.* **2018**, *3*, 18003.
[38] D. Meng, H. Fu, C. Xiao, X. Meng, T. Winands, W. Ma, W. Wei, B. Fan, L. Huo, N. L. Doltsinis, Y. Li, Y. Sun, Z. Wang, *J. Am. Chem. Soc.* **2016**, *138*, 10184–10190.
[39] D. Meng, G. Liu, C. Xiao, Y. Shi, L. Zhang, L. Jiang, K. Baldridge, Y. Li, J. Siegel, Z. Wang, *J. Am. Chem. Soc.* **2019**, *141*, 5402–5408.
[40] C. Schaack, A. Evans, F. Ng, M. Steigerwald, C. Nuckolls, *J. Am. Chem. Soc.* **2022**, *144*, 42–51.
[41] C. Wolf, *Chem. Soc. Rev.* **2005**, *34*, 595–608.
[42] We observe a second, long lived (≈44 ns), component in lifetime measurements when measuring at the red edge of the emission. Given the very small amplitude of this component, we safely assign the lifetime to a single component.
[43] T. Weng, G. V. Baryshnikov, C. Deng, X. Li, B. Wu, H. Wu, H. Ågren, Q. Zou, T. Zeng, L. Zhu, *Small* **2020**, *16*, 1906475.
[44] S. K. Pedersen, V. B. R. Pedersen, F. S. Kamounah, L. M. Broløs, G. V. Baryshnikov, R. R. Valiev, K. Ivaniuk, P. Stakhira, B. Minaev, N. Karaush-Karmazin, H. Ågren, M. Pittelkow, *Chem. Eur. J.* **2021**, *27*, 11609–11617.
[45] J. Gierschner, J. Shi, B. Milián-Medina, D. Roca-Sanjuán, S. Varghese, S. Park, *Adv. Opt. Mater.* **2021**, *9*, 2002251.
[46] M. Stolte, T. Schembri, J. Süß, D. Schmidt, A. Krause, M. O. Vysotsky, F. Würthner, *Chem. Mater.* **2020**, *32*, 6222–6236.
[47] S. K. Lee, Y. Zu, A. Herrmann, Y. Geerts, K. Müllen, A. J. Bard, *J. Am. Chem. Soc.* **1999**, *121*, 3513–3520.
[48] Y. Liang, Z. Xu, J. Xia, S.-T. Tsai, Y. Wu, G. Li, C. Ray, L. Yu, *Adv. Mater.* **2010**, *22*, E135–E138.
[49] S.-H. Liao, H.-J. Jhuo, Y.-S. Cheng, S.-A. Chen, *Adv. Mater.* **2013**, *25*, 4766–4771.
[50] Y. Sun, J. H. Seo, C. J. Takacs, J. Seifter, A. J. Heeger, *Adv. Mater.* **2011**, *23*, 1679–1683.
[51] J. Cao, S. Yang, *RSC Adv.* **2022**, *12*, 6966–6973.

Manuscript received: August 21, 2022
Accepted manuscript online: September 29, 2022
Version of record online: October 25, 2022